2017 IEEE/RSJ International Conference on Intelligent Robots and Systems (IROS)
September 24–28, 2017, Vancouver, BC, Canada

A high speed motion capture method and performance metrics for studying gaits on an insect-scale legged robot

Benjamin Goldberg, Neel Doshi, Kaushik Jayaram, Je-Sung Koh, and Robert J. Wood

***Abstract*— This paper develops a custom motion capture system that uses vision-based methods to rapidly and accurately track the body and leg position/orientation of a 1.43g legged microrobot, the Harvard Ambulatory MicroRobot (HAMR). Two new generalized metrics for quantifying locomotion performance are defined: amplitude-normalized stride correlation, and percent ineffective stance. Six different gaits are run on HAMR to validate the experimental setup and establish baseline performance. Furthermore, HAMR is compared with the cockroach, *Blaberus Discoidalis*, and with other legged robots. Future studies can leverage the experimental setup to study gait selection and transitions for small legged systems.**

I. Introduction

Detailed studies have been conducted on the biomechanics of locomotion in small animals, including cockroaches [1], geckos [2], and wood ants [3]. These studies have revealed that mechanics of running for animals that vary in leg morphology, leg number, and body size can be captured by simple, low-dimensional, physics-based models called templates [4].

Given the nascent phase of research on miniature legged robots, prior work has typically focused on the manufacturing and design aspects [5]. Some studies on legged robots, however, have begun exploring performance similarities and deviations from findings in animals. For example, SLIP dynamics in small-scale robots have been reported (e.g., DASH [6]) while others explain deviations from this model (e.g., Sprawlita [7] and VelociRoACH [8]). At even smaller scales, a recent study looked at the effect of varying the gait on a sub-2g robot that is externally actuated using magnetic fields [9].

One of the smallest and fastest legged robots is the Harvard Ambulatory MicroRobot (HAMR), an insect-scale quadrupedal robot. The design and manufacturing of HAMR has been explored by Baisch et al., and HAMR was shown to run at speeds above $44\,\mathrm{cm\,s^{-1}}$ – corresponding to 10 body lengths/second (BL/s) [10].

In prior tests with HAMR, qualitative evidence revealed that foot slippage and body oscillations have a substantial impact on the speed and efficiency of locomotion performance. As such, we develop new quantitative metrics that capture these effects. Furthermore, the experimental setup and metrics are used to measure the baseline performance of HAMR as we seek to establish it as a robust platform for studying hypotheses from biology (e.g., sensing and control architectures) that are challenging to test on animals.

These authors are with the John A. Paulson School of Engineering and Applied Sciences, Harvard University, Cambridge, MA 02138, USA, and the Wyss Institute for Biologically Inspired Engineering, Harvard University, Boston, MA, 02115, USA (email: bgoldberg,ndoshi,kjayaram,jskoh,rjwood@seas.harvard.edu)

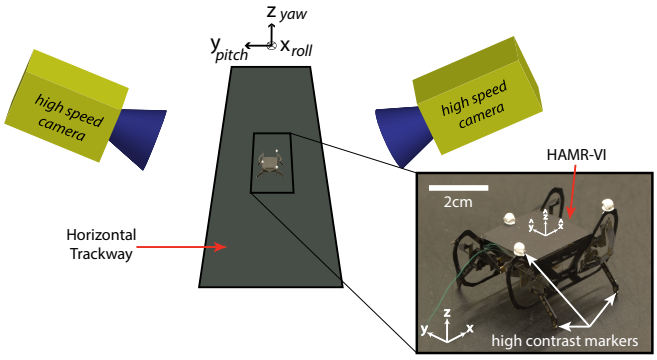

Fig. 1. Locomotion trackway for motion capture of the Harvard Ambulatory MicroRobot (HAMR). Two high speed cameras perform a reconstruction for the body and four feet of HAMR.

In Section II, we give an overview of the HAMR platform. Section III defines two new metrics: amplitude-normalized stride correlation (ANSC) and ineffective stance (IS) that capture the effects of body oscillations and foot slippage, respectively. Section IV motivates the need for developing a custom motion-capture arena and presents the high speed motion capture system (Fig. 1) used to conduct locomotion studies and validate the new metrics. Section V presents the results of six different gaits, and applies the new metrics to other legged systems to demonstrate their versatility. Finally, in Section VI we discuss how the methodology and metrics developed here can be used for gait selection in legged systems.

II. HAMR Overview

The most current version of HAMR, HAMR-VI, is a 1.43g quadruped with eight independently actuated degrees of freedom (DOFs). The PC-MEMS fabrication process and pop-up assembly techniques allow for fast and repeatable assembly of the complex leg transmissions (Fig. 2a) in HAMR despite its small scale [10]. Each DOF is driven by a piezoelectric actuator which allows HAMR to run at stride frequencies exceeding 100 Hz. Previously, speeds were measured for the trotting gait with a six-DOF version of HAMR, achieving a top speed of $44\,\mathrm{cm\,s^{-1}}$. In these studies, HAMR-VP was limited to three standard quadrupedal gaits (the walk, trot, and pace) due to the mechanical coupling between contralateral swing DOFs and, furthermore, the motion of the feet was not considered.

The current version of HAMR (HAMR-VI) described in [11] has the ability to independently control each of the

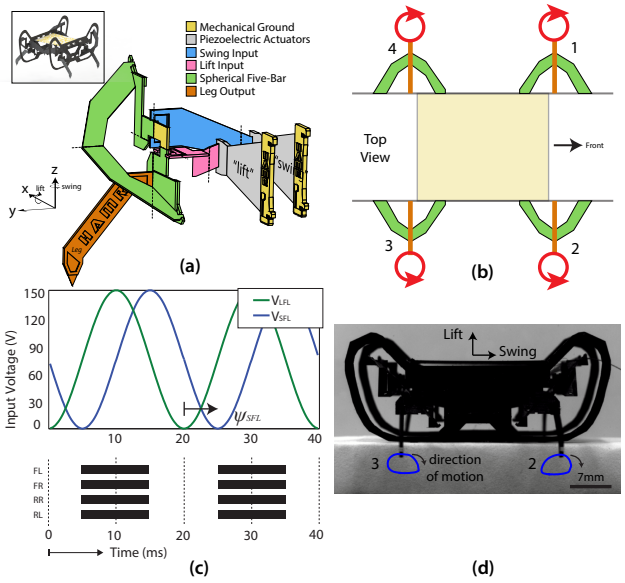

Fig. 2. a) Perspective view of the 2-DOF, single-leg, spherical five-bar transmission with lift and swing DOFs. b) Top view of whole robot with leg number convention. c) Example actuator input signals for a 50 Hz stride frequency and open-loop commanded footfall pattern for the pronk gait with shaded areas indicating stance phase. d) Side view with tracked leg trajectories for the front right and rear right legs.

eight DOFs. This makes HAMR-VI well suited to study the dynamics of legged locomotion at this scale, and motivates the need for a new, high resolution (100 µm) and high speed ($>$ 2000 Hz) experimental characterization technique. The baseline performance of HAMR-VI is described in Section V, however, the main contributions of this work are in the development of the experimental setup and performance analysis methods. A more comprehensive study of HAMR-VI locomotion and conclusions on principles of small scale legged running is the subject of a more detailed locomotion study in [12].

III. Metric Definition

In addition to common metrics such as speed, leg forces, and cost of transport, other metrics such as stability and foot kinematics are also important to consider. To further understand the underlying mechanics of legged locomotion, two new metrics are defined in the following subsections: ANSC and IS. The aim for these metrics is to compare gaits and identify regimes where body dynamics and foot slippage significantly affect locomotion.

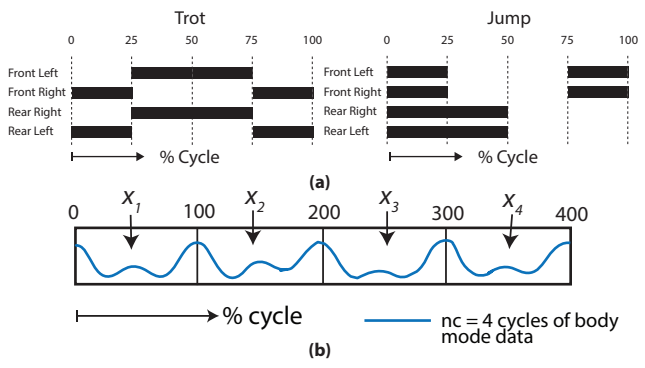

Fig. 3. (a) Open-loop commanded footfall patterns for two standard quadrupedal gaits: the trot (left) and jump (right). (b) Example of four cycles of segmented time-course body mode data (e.g. center of mass z-height) for calculating the covariance matrix in Eq. 1.

A. Amplitude-Normalized Stride Correlation (ANSC)

Stability is important to consider and, for this, there are formal definitions for hybrid dynamic running systems; for example, using Floquet analysis [13]. Other approaches for small scale runners look at static and dynamic stability [14], [15] or experimental metrics that compare the deviations in energy from stride to stride [16]. The proposed metric of ANSC is a measure of the amplitude and periodicity of body oscillations that can be used to inform a sense of stability. The strength of this analysis is that it does not require a detailed model and it is dimensionless, allowing for comparisons across length scales.

If in a limit cycle, the body modes (i.e., x-y-z-roll-pitch-yaw defined in Fig. 1) are expected to be periodic at the prescribed stride frequency or dominant observed frequency. As such, the time course data is segmented into a collection of cycles with period equal to the inverse of the dominant frequency (Fig. 3b). From this data, we compute a covariance matrix, $C \in \mathcal{R}^{nc \times nc}$ to measure periodicity at that frequency:

$$C = \frac{1}{\text{FPC}} \begin{bmatrix} (x_1)^T(x_1) & \dots & (x_1)^T(x_{nc}) \\ \vdots & \ddots & \vdots \\ (x_{nc})^T(x_1) & \dots & (x_{nc})^T(x_{nc}) \end{bmatrix} \quad (1)$$

Here x_i is the time-course data of one of the body modes for the ith stride, nc is the number of strides ($i = 1, \dots, nc$), and FPC (frames-per-cycle) is the number of data points collected per stride. To remove the effects of drift (or in the case of the x direction, forward locomotion), each of the x_i are computed by subtracting the best fit line from the raw data.

The covariance matrix is then normalized (Equation 2) so the auto-covariances (diagonal entries) equal one.

$$\text{P} = (D)^{-1} C (D)^{-1}, \qquad D = \sqrt{\text{diag}(C)} \quad (2)$$

We then compute the mean of the off-diagonal entries of P, i.e., the average correlation coefficient between cycles (r_m). Values range from -1 to 1, with a values close to 1 implying limit cycle behavior at the considered frequency. The ANSC of a body mode, s_m, is defined as r_m divided by the root-mean-square (RMS_m) magnitude of oscillation for that body mode. For body position modes, the quantity is normalized by the body length (L): $s_m^{xyz} = {}^{(r_m L)}/_{\text{RMS}_m}$ and for body angles, ANSC is: $s_m^{\theta\phi\psi} = {}^{(r_m)}/_{\text{RMS}_m}$.

As defined above, ANSC is dimensionless and while the lower bound of ANSC is zero, there is no upper bound as RMS oscillations can be arbitrarily small. However, relative comparisons can still be made; for example, a two-fold increase in ANSC can be due to either of the following (or

some partial combination): doubling the cyclical correlation, doubling the length scale (i.e., a larger body), or halving the magnitude of RMS body oscillations. Baseline measures of ANSC in Section V-C give an idea of typical ranges for legged systems. Furthermore, this metric can be applied to systems beyond those explored in this paper where periodicity arises autonomously and is not explicitly enforced (e.g. MABEL and ATRIAS [17], [18]) by using a discrete Fourier transform to determine the frequency of the limit cycle (the dominant observed frequency).

B. Ineffective stance

Foot slippage is often observed during locomotion involving perturbations or on complex terrain. A normalized metric for foot slippage, however, has not yet been established. Prior studies looking at foot slippage have used metrics such as *stride success ratio* [19] and *step displacement* [20]. These metrics work well when the amount of foot slippage is binary (foot does or does not slip) or aggregated over all of the legs. However, these measures do not capture variations between individual legs in a quantitative way. Therefore, we propose a duration based metric, IS, to quantify deviations from an idealized leg trajectory in the sagittal plane (Fig. 4) based on the leg position, $\tilde{\mathbf{p}}$, and velocity in the world and body frame, $\tilde{\mathbf{v}}_\mathbf{w}$ and $\tilde{\mathbf{v}}_\mathbf{b}$, respectively*. IS can be used to measure the effect of these deviations on locomotion performance (e.g. speed).

Consequently, the main aim of IS is to quantify the percentage of the gait cycle that is neither an ideal "swing" nor "stance". As such, the gait cycle is considered to consist of three categories: swing, stance, and ineffective stance. During a gait cycle, the amount of time for swing, stance, and ineffective stance can be described as the following:

> ***Swing***: Amount of time the foot is above the ground ($p_{wz} > 0$) *and* has a positive forward velocity a body-fixed frame ($v_{bx} > 0$).
>
> ***Stance***: Amount of time the foot is planted on the ground ($p_{wz} = 0$) *and* has zero velocity relative to a fixed world frame ($v_{wx} = 0$).
>
> ***Ineffective Stance***: Amount of time that the leg is slipping on the ground ($p_{wz} = 0 \,\&\, v_{wx} < 0$) *or* swinging backwards in air ($p_{wz} > 0 \,\&\, v_{bx} < 0$).

Quantitatively, these categories make up the total time, T_{total}, of the cycles(s) of the gait being analyzed:

$$T_{\text{total}} = T_{\text{swing}} + T_{\text{stance}} + T_{\text{IS}} \tag{3}$$

As a percentage IS can range from 0-100%, where $\text{IS} = {}^{T_{\text{IS}}}/_{T_{\text{total}}}$. When the leg is always in either swing or stance phase, IS=0%. This would result in maximum forward velocity for an ideal legged system. On the other hand, IS=100% implies the leg motion deviates from the desired trajectory throughout the complete gait cycle; for example, when relative motion occurs between the foot and the ground substrate when in contact or if the leg swings back in air. In these cases, forward locomotion is still possible, but is likely to be reduced.

*Boldface and vector notation indicates 3D vectors in Cartesian coordinates.

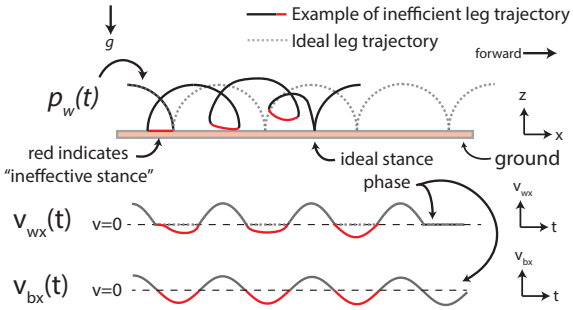

Fig. 4. Qualitative example of a foot trajectory as a function of time, t, with a non-zero level of ineffective stance.

These descriptions can be calculated numerically with the following equations:

$$T_{\text{swing}} = \frac{\sum_{k=1}^{L} \Big(p_{wz}(k) > 0 \;\&\; v_{bx}(k) \geq 0 \Big)}{L} T_{\text{total}} \tag{4}$$

$$T_{\text{stance}} = \frac{\sum_{k=1}^{L} \Big(p_{wz}(k) = 0 \;\&\; \tilde{\mathbf{v}}_\mathbf{w}(k) = \tilde{\mathbf{0}} \Big)}{L} T_{\text{total}} \tag{5}$$

where L is number of data points captured. In an experimental implementation, these calculations can be sensitive to measurement errors, therefore a 10% threshold (obtained by trial and error) should be used to determine whether or not the foot is on the ground ($p_{wz} = 0$) and the velocity is zero ($\tilde{\mathbf{v}}_\mathbf{w} = \tilde{\mathbf{0}}$).

Ineffective stance is measured for each of the legs but can be averaged to get a single measure of ineffective stance for the whole system, $\overline{\text{IS}}$. Additionally, this ineffective stance definition can be extended to systems that have continuous rotary motion (e.g. wheeled vehicles) with slight modifications. Ineffective stance for a wheeled system is when the wheel has an instantaneous velocity greater than the body velocity, as this implies that the instantaneous contact point has a non-zero velocity (the wheel is skidding).

IV. Locomotion Reconstruction

In order to compute the metrics proposed above, we require accurate reconstructions of the body and foot positions to observe slippage. Specifically, for studies on HAMR, an operating volume of $12\,\text{cm} \times 6\,\text{cm} \times 5\,\text{cm}$ is needed to capture at least 10 strides and ensure observed motion is not transient. Furthermore, a frame rate of 1500-2500 frames per second is desired to capture at least 30 frames per stride to reconstruct continuous motion with stride frequencies up to $65\,\text{Hz}$. Finally, markers on the feet need to be less than $0.5 \times 0.5 \times 0.5\,\text{mm}$ and $1\,\text{mg}$ in order to not hinder locomotion.

Motion capture systems, both commercial and custom, previously used for locomotion reconstruction at small scales

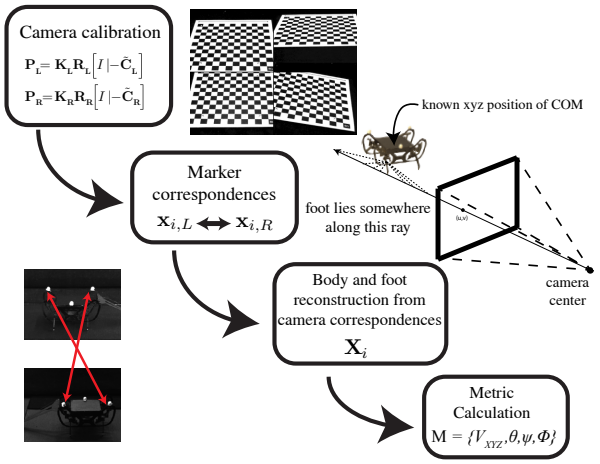

Fig. 5. Flowchart of the reconstruction process. Cameras are calibrated before running trials. Tracking, reconstruction and metric calculation is done in post-processing steps.

can only detect areas of high reflectance, have low frame rates (< 1000 fps), low resolution (and thus require relatively large markers), and/or constrain locomotion by limiting the type of substrates ([21], [22], [23]). In order to overcome these restrictions, we develop the custom motion capture system described below.

A. Measurement System Overview

A schematic of the locomotion trackway and motion capture arena is shown in Fig. 1. There are two high speed cameras (Vision Research, Phantom v7.3) mounted on either side of the robot sagittal plane. The robot has three spherical markers coated in white-out that are rigidly affixed to the body. Additionally, there is a single white dot painted onto the side of each foot of the robot for high contrast to the black running surface carbon fiber chassis. The number of frames per second (fps) for the cameras is set to $30\times$ the stride frequency. At the highest tested stride frequency of 65 Hz, this corresponds to 1950 fps. Faster capture rates are possible up to the camera's peak frame rate of 6688 fps. Signal generation for HAMR runs at 5 kHz using a MATLAB xPC environment (MathWorks, MATLAB R2015b). The robot runs on a smooth cardstock surface and each trial is conducted until a straight run occurs. The following sections describe the motion capture methodology in more detail.

B. Stereo Camera Reconstruction Workflow

The flowchart in Fig. 5 shows the steps required to obtain the final locomotion reconstruction. First, the cameras are calibrated with a checkerboard pattern. Videos are then taken of the robot running and are tracked off-line with custom tracking scripts in MATLAB. Post processing stereo reconstruction for the body is performed and is used to inform the subsequent foot reconstruction. While the body reconstruction is relatively straight forward using the MATLAB computer vision toolbox, a more involved foot reconstruction is required due to occlusions and to keep the number of cameras required to a minimum.

C. Foot Kinematics

The ability to accurately track four feet with only two cameras is one of the main contributions of this paper. Since only two cameras are used, each foot is only seen in one camera and stereo triangulation of the feet is not possible. Instead, reconstruction is performed by tracking the body position first and leveraging the known kinematics of the HAMR transmission. A schematic of the foot reconstruction method is shown in Fig. 6. Specifically, the foot lies on a sphere with the center at the spherical five-bar center, $\vec{b}$, fixed to the body. This can be computed in the world frame as follows:

$$\tilde{\mathbf{b}} = \mathrm{R}\tilde{\mathbf{c}}_\mathrm{o} + \tilde{\mathbf{X}}_\mathrm{COM} \tag{6}$$

where R is the 3D rotation matrix that describes the orientation of the robot in the world frame, $\vec{c}_\mathrm{o}$ is the vector from the center of mass to $\vec{b}$ in the body frame, and $\vec{X}_\mathrm{COM}$ is the position of the center of mass in the world frame. The position of the foot in the world, $\tilde{\mathbf{f}}$, is the intersection of the spherical surface parameterized by l (leg radius) and $\tilde{\mathbf{b}}$, with the ray defined by the camera center and the projection of the foot onto the image plane, $\tilde{\mathbf{p}}(\lambda)$. This intersection can be defined as:

$$||\tilde{\mathbf{p}}(\lambda) - \tilde{\mathbf{b}}||_2^2 - l^2 = 0 \tag{7}$$

The desired solution for the position of the foot is: $\tilde{\mathbf{f}} = \tilde{\mathbf{p}}(\lambda^*)$ where λ^* is the value of the parameterization that minimizes the quantity in Eq. 7. Writing the norm-squared in vector form, equation 7 becomes:

$$(\tilde{\mathbf{p}}(\lambda) - \tilde{\mathbf{b}})^T(\tilde{\mathbf{p}}(\lambda) - \tilde{\mathbf{b}}) - l^2 = 0 \tag{8}$$

The ray through the image plane, $\tilde{\mathbf{p}}(\lambda)$ can be obtained by back-projecting the tracked foot marker in (u, v) pixel coordinates given the camera matrix, P and camera center C and then normalizing into Cartesian coordinates:

$$\tilde{\mathbf{p}}(\lambda) = \underbrace{P^\dagger \begin{bmatrix} u \\ v \\ 1 \end{bmatrix}}_{r} + \lambda \mathrm{C} \tag{9}$$

$P^\dagger$ is the pseudo-inverse of the camera matrix. Normalizing into Cartesian coordinates gives:

$$\tilde{\mathbf{p}}(\lambda) = \frac{\tilde{\mathbf{r}} + \lambda\tilde{\mathbf{C}}}{r_4 + \lambda} \tag{10}$$

where $\tilde{\mathbf{r}}$ is the first three entries of the homogeneous vector r, and r_4 is the last entry of r. $\tilde{\mathbf{C}}$ and C are the camera center in Cartesian and homogeneous coordinates, respectively, with C_x, C_y, C_z being the 3-D position of the camera center.

$$\tilde{\mathbf{C}} = \begin{bmatrix} C_x \\ C_y \\ C_z \end{bmatrix}, \mathrm{C} = \begin{bmatrix} C_x \\ C_y \\ C_z \\ 1 \end{bmatrix}$$

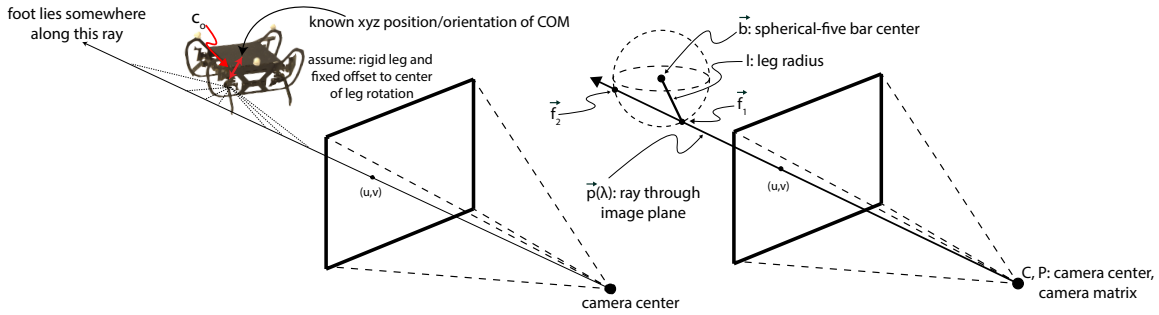

Fig. 6. Schematic of the foot reconstruction strategy.

TABLE I
BODY RECONSTRUCTION WITH 15 mm TRANSLATIONS (N=3)

	Reconstruction Error	
	mm	%
fore-aft (x)	0.45 ± 0.07	3.0
lateral (y)	0.64 ± 0.06	4.3
vertical (z)	0.58 ± 0.10	3.9

Substituting equation 6 and 10 into equation 8, gives a quadratic equation for λ of the form $a\lambda^2 + b\lambda + c = 0$ and a solution for λ can be found analytically. After performing the substitution, a, b, and c are determined to be the following:

$$a = \tilde{\mathbf{b}}^T\tilde{\mathbf{b}} - l^2 - 2\tilde{\mathbf{C}}^T\tilde{\mathbf{b}} + \tilde{\mathbf{C}}^T\tilde{\mathbf{C}}$$
$$b = 2r_4(\tilde{\mathbf{b}}^T\tilde{\mathbf{b}} - l^2) - 2(r_4\tilde{\mathbf{C}}^T\tilde{\mathbf{b}} + \tilde{\mathbf{r}}^T\tilde{\mathbf{b}}) + 2\tilde{\mathbf{r}}^T\tilde{\mathbf{C}}$$
$$c = (\tilde{\mathbf{b}}^T\tilde{\mathbf{b}} - l^2)r_4^2 - 2r_4\tilde{\mathbf{r}}^T\tilde{\mathbf{b}} + \tilde{\mathbf{r}}^T\tilde{r}$$

The solution, λ^*, is the solution for λ that is closest to the camera center. Due to predominant motion along the camera axis, the displacement of the foot in the $\hat{y}$ (body lateral direction) is more difficult to resolve. For the metrics in this paper, however, only the lift and swing displacements of the foot are used ($d_{\hat{x}}$ and $d_{\hat{z}}$, respectively). An evaluation of the foot reconstruction accuracy is described in Section V-A.

V. RESULTS

A. Motion Capture System Evaluation

The following sections evaluate the accuracy of the motion capture system for both the body and foot reconstruction.

a) Body Reconstruction Accuracy: To quantify the accuracy of the rigid body reconstruction, the robot is placed on a 3-DOF micromanipulation stage and is translated in 15 mm increments. Table I quantifies the body reconstruction error, which is less than 5% in each direction. These small errors mainly arise due to variations in lighting and marker detection, as the reprojection error of the calibration is consistently below 0.2 pixels (28 µm).

b) Foot Reconstruction Accuracy: The accuracy of the custom foot reconstruction is evaluated by running the robot suspended in air and comparing the reconstructed foot trajectory against the foot trajectory from a stereo foot reconstruction conducted in [11]. The swing DOF displacement, d_x, in the custom foot reconstruction is only 9% greater compared to the baseline from [11]. This is within the bounds of manufacturing and measurement errors. The other DOF, however, is not as accurate due to foreshortening effects of the camera angle with respect to the foot trajectory. The foot lift, d_z, is underestimated by the custom foot reconstruction by 31%. Phase information, however, is preserved with this strategy and future work will improve the lift DOF reconstruction by implementing a Bayesian estimator [24] and optimizing the angle of the cameras.

B. Metric Comparison for Six Gaits

Six sample trials are analyzed to highlight how the metrics defined in Section III can be used to capture differences between gaits. In this section, two gaits, the trot and jump, are compared for five metrics, including the two new metrics, IS and ANSC. The reported IS is an average of all legs and the reported ANSC is an average of the x, z, and pitch ANSC, to account for each DOF of the sagittal plane. A summary of these metrics is shown in Table II.

The fastest gait is the 65 Hz jump (shown in the supplemental video) with a speed of 10.6 BL s^{-1} (48.0 cm s^{-1}). This gait has the highest ANSC for HAMR of 92. The gait with the lowest ANSC for HAMR (15) is the 15 Hz jump. This gait has large peak-to-peak oscillations and is highly variable from cycle to cycle. At higher stride frequencies, however, the jump begins to stabilize, indicated by the increased ANSC at the 40 and 65 Hz jump gaits.

The gait with the lowest ineffective stance is the 10 Hz trot which has the highest normalized speed (average distance traveled per step) of 9.5 mm/stride. One hypothesis for this result is that the footfall timings consistently align with the body resonant modes, which have been previously identified to be around the 10 Hz stride frequency regime [10]. It is also expected that ineffective stance will increase with increasing stride frequency due to increased foot velocities and a constant coefficient of friction. All gaits for HAMR have moderately high levels of IS ranging from 25-39%. This is likely due to the smooth cardstock running surface allowing the feet to slip, even at low stride frequencies such as during the 1 Hz trot with (IS =35%).

C. Metric comparison to other legged systems

The newly defined metrics are calculated using kinematic data from three other legged systems: the flying monkey (4.3 g), the commercial version of DASH (29.9 g), and the *Blaberus discoidalis* cockroach (2.06 g) ([25], [6], [26]). A summary of the performance metrics are shown in Table

TABLE II

INPUT CONDITIONS AND CALCULATED METRICS FOR SIX HAMR GAITS

Input Conditions			**Performance Metrics**			
Platform	Gait	Stride Frequency (Hz)	Speed ($\mathrm{BL\,s^{-1}}$)	Normalized Speed ($^{\mathrm{mm}}/_{\mathrm{stride}}$)	Ineffective stance ($\overline{\mathrm{IS}}$, %)	ANSC
HAMR-VI	Trot	1	0.2	8.5	35	89
HAMR-VI	Trot	10	2.1	9.5	25	48
HAMR-VI	Trot	65	9.1	6.2	38	42
HAMR-VI	Jump	15	1.8	5.3	26	15
HAMR-VI	Jump	40	6.9	7.7	38	60
HAMR-VI	Jump	65	10.6	7.4	39	92

TABLE III

CROSS PLATFORM COMPARISON

	Normalized Performance Metrics			
Platform*	Stride Frequency (Hz)	Normalized Speed ($^{\mathrm{BL}}/_{\mathrm{stride}}$)	Ineffective stance ($\overline{\mathrm{IS}}$, %)	ANSC
HAMR-VI‡	1-65	0.16	34	67
Flying Monkey	52	0.18	56	21
DASH	18.7	0.35	60	11
Blaberus discoidalis	14.9	0.93	5	94

*Body Length: HAMR-VI (45.1mm), Flying Monkey ($40.0\,\mathrm{mm}$), DASH ($118\,\mathrm{mm}$), *Blaberus discoidalis* ($41.7\,\mathrm{mm}$)

‡ Reported values are the mean of the six trials.

III[†]. Compared to HAMR, the flying monkey and DASH robots have relatively low ANSC. Qualitatively, this means that these robots tend to bounce higher and more irregularly than the tuned gaits of HAMR. In the case of DASH and the flying monkey, low ANSC also leads to higher levels of ineffective stance. Speeds of 9.2 and 6.5 $\mathrm{BL\,s^{-1}}$ (corresponding to 0.18 and 0.35 BL/stride) are achieved for the flying monkey and DASH. However, the lower stability (23 and 5, respectively) and high ineffective stance (56% and 60%, respectively) suggests that higher speeds would be possible with improvements to the gaits and foot contacts.

Blaberus discoidalis is the fastest of the legged systems relative to body length in the tests considered here at $13.8\,\mathrm{BL\,s^{-1}}$ and also has the highest ANSC of 139 and lowest ineffective stance of 5%. This suggests that the metrics are capturing foot stance and steady state behavior appropriately since it is known from the biological experiments that both are true [27].

VI. CONCLUSION AND FUTURE WORK

The motion capture system developed here is high speed and accurate with sub millimeter resolution. The off-line tracking is quick ($\sim 1\,\mathrm{min}$ per trial) and reliable ($< 5\%$ body reconstruction error and a minimum detection resolution of $50\,\mu\mathrm{m}$ for the feet). The metrics defined here capture relative performance differences between commanded open-loop gait patterns and can also be useful to compare across platforms. The development and validation of the experimental setup and metrics presented here will be helpful to improve the design and control of legged robots at the insect-scale. An extension of this work that leverages an understanding of high frequency gaits on HAMR to achieve high speed feedback control is discussed in [28].

Overall, the metrics introduced here can be used for performing an experimental optimization of gaits; for example, maximizing ANSC or minimizing ineffective stance. Furthermore, the results of this work might be of interest to biologists who have hypotheses about insect-scale locomotion and we contend such hypotheses can now be tested in a controlled manner on HAMR, an at-scale platform.

One limitation of this study is that the relationship between the input actuator signals (nominal gait) and the observed footfall patterns varies with gait and stride frequency. This topic, along with ground reaction force measurements and a more detailed analysis of gaits is explored in [12].

Beyond running straight on flat terrain, this methodology can be applied to other locomotion scenarios such as experiments on perturbation rejection, control, and climbing. The ineffective stance and stability metrics will give a fundamental understanding of why certain gaits might perform better than others in studies beyond open-loop, level ground running. Future work should compare the new stability analysis methods with existing metrics (e.g. Floquet analysis) in order to achieve more robust locomotion on uneven terrains or in the presence of perturbations.

While the results in this paper only covered a handful of trials, the strength of the setup presented here is that a large number of trials can be run and processed very easily. In the future, this will ultimately be a very useful tool to study varying gaits on small-scale biologically inspired robots. A large number of input parameters can be varied and evaluated for many different metrics.

ACKNOWLEDGMENTS

Thank you to all members of the Microrobotics Lab for valuable discussions. Thanks to Prof. Todd Zickler for help starting this work during a class project in his Computer Vision class. This work is partially funded by the Wyss Institute for Biologically Inspired Engineering and the National Science Foundation. This material is based upon work supported by the National Science Foundation Graduate Research Fellowship under Grant Number DGE1144152. Any opinion, findings, and conclusions or recommendations expressed in this material are those of the authors and do not necessarily reflect the views of the National Science Foundation. In addition, the prototypes were enabled by

[†]In these comparisons, the running surface is flat cardstock with the exception of the flying monkey which runs on 240 grit sandpaper.

equipment supported by the ARO DURIP program (award #W911NF-13-1-0311)

REFERENCES

[1] R. J. Full and M. S. Tu, "Mechanics of a rapid running insect: two-, four-and six-legged locomotion," *Journal of Experimental Biology*, vol. 156, no. 1, pp. 215–231, 1991.

[2] J. Chen, A. Peattie, K. Autumn, and R. Full, "Differential leg function in a sprawled-posture quadrupedal trotter," *Journal of Experimental Biology*, vol. 209, no. 2, pp. 249–259, 2006.

[3] L. Reinhardt, T. Weihmann, and R. Blickhan, "Dynamics and kinematics of ant locomotion: do wood ants climb on level surfaces?" *The Journal of experimental biology*, vol. 212, no. 15, pp. 2426–2435, 2009.

[4] R. J. Full and D. E. Koditschek, "Templates and anchors: neuromechanical hypotheses of legged locomotion on land," *Journal of Experimental Biology*, vol. 202, no. 23, pp. 3325–3332, 1999.

[5] D. W. Haldane, C. S. Casarez, J. T. Karras, J. Lee, C. Li, A. O. Pullin, E. W. Schaler, D. Yun, H. Ota, and A. Javey, "Integrated manufacture of exoskeletons and sensing structures for folded millirobots," *Journal of Mechanisms and Robotics*, vol. 7, no. 2, p. 021011, 2015.

[6] P. Birkmeyer, K. Peterson, and R. S. Fearing, "DASH: A dynamic 16g hexapedal robot," in *IEEE/RSJ Intl. Conf. on Intelligent Robots and Systems*. IEEE, 2009, pp. 2683–2689.

[7] S. A. Bailey, J. G. Cham, M. R. Cutkosky, and R. J. Full, "Comparing the locomotion dynamics of the cockroach and a shape deposition manufactured biomimetic hexapod," in *Experimental Robotics VII*. Springer, 2001, pp. 239–248.

[8] D. W. Haldane and R. S. Fearing, "Running beyond the bio-inspired regime," in *Robotics and Automation (ICRA), 2015 IEEE International Conference on*. IEEE, 2015, pp. 4539–4546.

[9] R. St Pierre and S. Bergbreiter, "Gait exploration of sub-2 g robots using magnetic actuation," *IEEE Robotics and Automation*, 2016.

[10] A. T. Baisch, O. Ozcan, B. Goldberg, D. Ithier, and R. J. Wood, "High speed locomotion for a quadrupedal microrobot," *The International Journal of Robotics Research*, pp. 1063–1082, 2014.

[11] N. Doshi, B. Goldberg, R. Sahai, N. Jafferis, D. Aukes, and R. J. Wood, "Model driven design for flexure-based microrobots," in *Intelligent Robots and Systems (IROS), 2015 IEEE/RSJ International Conference on*. IEEE, 2015, pp. 4119–4126.

[12] B. Goldberg, N. Doshi, K. Jayaram, and R. Wood, "Gait studies for a quadrupedal microrobot reveal contrasting running templates in two frequency regimes," *Bioinspiration & Biomimetics*, vol. 12, no. 4, 2017.

[13] S. H. Strogatz, *Nonlinear dynamics and chaos: with applications to physics, biology, chemistry, and engineering*. Westview press, 2014.

[14] L. Ting, R. Blickhan, and R. Full, "Dynamic and static stability in hexapedal runners." *Journal of Experimental Biology*, vol. 197, no. 1, pp. 251–269, 1994.

[15] R. J. Full, T. Kubow, J. Schmitt, P. Holmes, and D. Koditschek, "Quantifying dynamic stability and maneuverability in legged locomotion," *Integrative and comparative biology*, vol. 42, no. 1, pp. 149–157, 2002.

[16] D. W. Haldane, K. C. Peterson, F. L. G. Bermudez, and R. S. Fearing, "Animal-inspired design and aerodynamic stabilization of a hexapedal millirobot," in *Robotics and Automation (ICRA), 2013 IEEE International Conference on*. IEEE, 2013, pp. 3279–3286.

[17] K. Sreenath, H.-W. Park, I. Poulakakis, and J. W. Grizzle, "A compliant hybrid zero dynamics controller for stable, efficient and fast bipedal walking on mabel," *The International Journal of Robotics Research*, vol. 30, no. 9, pp. 1170–1193, 2011.

[18] A. Ramezani, J. W. Hurst, K. A. Hamed, and J. W. Grizzle, "Performance analysis and feedback control of atrias, a three-dimensional bipedal robot," *Journal of Dynamic Systems, Measurement, and Control*, vol. 136, no. 2, p. 021012, 2014.

[19] K. Jayaram and R. J. Full, "Cockroaches traverse crevices, crawl rapidly in confined spaces, and inspire a soft, legged robot," *Proceedings of the National Academy of Sciences*, vol. 113, no. 8, pp. E950–E957, 2016.

[20] N. Mazouchova, P. B. Umbanhowar, and D. I. Goldman, "Flipper-driven terrestrial locomotion of a sea turtle-inspired robot," *Bioinspiration & biomimetics*, vol. 8, no. 2, p. 026007, 2013.

[21] L. M. Theunissen and V. Dürr, "Insects use two distinct classes of steps during unrestrained locomotion," *PLoS ONE 8(12): e85321.*, 2013.

[22] J. D. Crall, N. Gravish, A. M. Mountcastle, and S. A. Combes, "Beetag: a low-cost, image-based tracking system for the study of animal behavior and locomotion," *PloS one*, vol. 10, no. 9, p. e0136487, 2015.

[23] C. S. Mendes, I. Bartos, Z. Márka, T. Akay, S. Márka, and R. S. Mann, "Quantification of gait parameters in freely walking rodents," *BMC biology*, vol. 13, no. 1, p. 50, 2015.

[24] A. J. Spence, S. Revzen, J. Seipel, C. Mullens, and R. J. Full, "Insects running on elastic surfaces," *Journal of Experimental Biology*, vol. 213, no. 11, pp. 1907–1920, 2010.

[25] J.-S. Koh, D. M. Aukes, B. Araki, S. Pohorecky, Y. Mulgaonkar, M. T. Tolley, V. Kumar, D. Rus, and R. J. Wood, "A modular folded laminate robot capable of multi modal locomotion," in *International Symposium on Experimental Robotics (ISER 2016), Tokyo, Japan, Oct., 2016*.

[26] R. J. Full and M. S. Tu, "Mechanics of six-legged runners," *Journal of experimental biology*, vol. 148, no. 1, pp. 129–146, 1990.

[27] S. Revzen, S. A. Burden, T. Y. Moore, J.-M. Mongeau, and R. J. Full, "Instantaneous kinematic phase reflects neuromechanical response to lateral perturbations of running cockroaches," *Biological cybernetics*, vol. 107, no. 2, pp. 179–200, 2013.

[28] B. Goldberg, N. Doshi, and R. J. Wood, "High speed trajectory control using an experimental maneuverability model for an insect-scale legged robot," *2017 IEEE International Conference on Robotics and Automation (ICRA)*, 2017.